EBioMedicine 59 (2020) 102958

Contents lists available at ScienceDirect

EBioMedicine

journal homepage: www.elsevier.com/locate/ebiom

Review

Nanoparticle delivery *in vivo*: A fresh look from intravital imaging

Qiaoya Lin, Parinaz Fathi, Xiaoyuan Chen*

Laboratory of Molecular Imaging and Nanomedicine, National Institute of Biomedical Imaging and Bioengineering, National Institutes of Health, Bethesda, MD 20892, USA

ARTICLE INFO

Article History:
Received 4 June 2020
Revised 30 July 2020
Accepted 31 July 2020
Available online xxx

Keywords:
Endothelial cells
Neutrophils
Macrophages
Enhanced permeability and retention (EPR)
Intravital microscopy (IVM)

ABSTRACT

Nanomedicine has proven promising in preclinical studies. However, only few formulations have been successfully translated to clinical use. A thorough understanding of how nanoparticles interact with cells *in vivo* is essential to accelerate the clinical translation of nanomedicine. Intravital imaging is a crucial tool to reveal the mechanisms of nanoparticle transport *in vivo*, allowing for the development of new strategies for nanomaterial design. Here, we first review the most recent progress in using intravital imaging to answer fundamental questions about nanoparticle delivery *in vivo*. We then elaborate on how nanoparticles interact with different cell types and how such interactions determine the fate of nanoparticles *in vivo*. Lastly, we discuss ways in which the use of intravital imaging can be expanded in the future to facilitate the clinical translation of nanomedicine.

1. Introduction

Nanoparticle (NP) delivery systems are widely utilized in biomedical applications to improve human health through disease prevention, diagnosis, and treatment. A wide variety of nanoparticles are being investigated preclinically. However, only a handful of anticancer nanoformulations, predominantly in liposomal form, have been approved by the Food and Drug Administration (FDA) or the European Medicines Agency (EMA) [1]. A thorough understanding of how nanoparticles interact with tissues and cells *in vivo* is essential to accelerate the clinical translation process [2, 3].

Intravital imaging, the imaging of live animals at microscopic resolution, is gaining increasing attention in biomedicine because it can provide multicolour spatiotemporal information at single-cell resolution in a variety of organs *in vivo*. In addition to the early imaging of lymph nodes [4, 5] and recent visualization of mouse embryos [6], intravital imaging has become a critical tool to reveal the novel mechanism of nanoparticle transport in the tumour microenvironment [7–9]. Here, we review recent progress on the use of intravital imaging in answering fundamental questions about nanoparticle delivery *in vivo*.

2. Intravital imaging to answer fundamental questions about nanoparticle delivery *in vivo*

2.1. Intravital microscopy (IVM) imaging of nanoparticle-neutrophil interactions

Systemic delivery is one of the most common routes to reach target sites in the body. When nanoparticles are intravenously administered, the first type of cells they will most likely encounter are the cells circulating in the bloodstream. Neutrophils are the most abundant circulating leukocytes in mice and humans [10].

Intravital imaging enables dynamic recording of direct interactions between NPs and neutrophils, which is critical for identifying the role of neutrophils in NP delivery. For example, Naumenko et al. used IVM to compare the accumulation dynamics of Cy5-labelled magnetic nanoparticles, shaped as cubes and clusters, in murine breast cancer (4T1) and colon cancer (CT26) models [11]. Both NPs were mainly captured by neutrophils ($CD11c^+Ly6G^+$ double-positive cells) in the tumour vasculature immediately after injection. Analysis of cell behaviour revealed that most of the NP-bound neutrophils were actively crawling in the tumour vessels, while only approximately 25% of cells adhered to the endothelium. Intravital imaging also revealed that NP-laden neutrophils extravasated through the endothelium in tumour tissue within 10–30 min after injection. Neither the cell capture nor the extravasation pattern differed between cubes and clusters. Nevertheless, the neutrophil-dependent delivery route was more impactful for shorter-circulating cubes (less than 5 min) than longer-circulating nanoclusters. Neutrophil-mediated

* Corresponding author.
E-mail address: chen9647@gmail.com (X. Chen).

https://doi.org/10.1016/j.ebiom.2020.102958

transport was also shown to be dependent on tumour type, and was more efficient in 4T1 tumours, which were more neutrophil-rich, than CT26 tumours [11].

Others have taken advantage of NP-neutrophil interactions to develop an activated neutrophil delivery strategy. Bovine serum albumin (BSA)-modified carboxylated polystyrene nanoparticles with a size of 130 nm were able to specifically recognize activated neutrophils, not resting neutrophils [12]. IVM imaging demonstrated that activated neutrophils (labelled by Alexa Fluor-488-labelled anti-mouse Gr-1 antibody) internalized Cy5-labelled albumin NPs within 30 min post-injection in mice; the activated neutrophils then transported NPs across the blood vessel barrier after intrascrotal administration of TNF-α. Moreover, anti-CD11b antibody-decorated gold nanorods (NP-CD11b) were developed to target activated neutrophils [13]. The movement of NP-CD11b into lung carcinoma tumours was mediated by neutrophil infiltration induced by photosensitization. Neutrophil infiltration enhanced nanoparticle delivery and cancer therapy efficacy. Aside from the chemical conjugation methods described above, Wang et al. applied nitrogen cavitation to rapidly destroy activated neutrophils and produce cell membrane vesicles. [14]. Such vesicles were able to behave like intact neutrophils and bind selectively to inflamed vasculature through integrin β2 on the vesicle surface and intercellular adhesion molecule 1 (ICAM-1) on the surface of activated endothelial cells. When loaded with NF-κB inhibitor, the systemically administered nanovesicles markedly mitigated mouse acute lung inflammation. The same group also reviewed the use of IVM to image nanotherapeutics in inflamed vasculature in detail [15]. As shown in summary Table 1, nanoparticles utilized in intravital imaging of neutrophils were all negatively charged and greater than 100 nm in size. Additionally, neutrophils were more impactful in the delivery of cube-shaped Fe_3O_4 NPs than in the delivery of cluster-shaped NPs. Thus, the speed of NP internalization within neutrophils is an important consideration for future use of the neutrophil-dependent delivery route.

2.2. IVM imaging of NP-Monocyte/Macrophage interactions

Beyond neutrophils, other myeloid cells, such as monocytes/macrophages, which belong to the mononuclear phagocyte system (MPS) also play a pivotal role in nanoparticle delivery [16,17].

2.2.1. Monocytes in blood

Gambhir's group found that Cy5-labelled PEGylated single-walled carbon nanotubes (SWNTs) were almost exclusively taken up by Ly-6C^{hi} inflammatory monocytes and delivered to tumours in mice. This monocyte-mediated delivery served as a "trojan horse" and accounted for approximately 25% of SWNT delivery to the tumour site [7]. Building upon these observations, Flores et al. loaded SWNTs with a chemical inhibitor of the antiphagocytic CD47-SIRPα signalling axis, which plays an important role in atherosclerosis. The selective uptake of these SWNTs in Ly-6C^{hi} inflammatory monocytes led to their subsequent delivery to diseased arteries, where Ly-6C^{hi} cells typically differentiate into lesional macrophages. This approach enabled the activation of lesional phagocytosis, thus preventing atherosclerosis [18]. For circulating monocytes in the bloodstream, there exists another subset of monocytes, Ly6C^{lo} monocytes, which have been shown to play an immunosuppressive role [19]. Jung et al. performed intravital imaging in syngeneic SL4 colorectal cancer (CRC) tumour-bearing Cx3cr1$^{gfp/+}$mice with abdominal imaging windows. In this study, Ly6C^{lo} monocytes were labelled with EGFP, and the blood vessels were labelled with TRITC-dextran. The images showed the flowing, crawling, and rolling of Ly6C^{lo} monocytes inside blood vessels, as well as CX3CR1^{+}Ly6C^{lo} monocytes undergoing extravasation in the SL4 tumour. Thus, it revealed that CX3CR1 is crucial for Ly6C^{lo} monocyte transmigration across the endothelium in murine CRC models. Gene therapy using a clinically relevant nanoparticle (7C1) [20] that targeted endothelial cells and delivered siRNA against CX3CL1 reduced Ly6C^{lo} monocyte recruitment and improved the outcome of anti-VEGFR2 therapy in mouse SL4 CRCs [19].

2.2.2. Kupffer cells in the liver

Monocytes differentiate into macrophages in a variety of tissues. Kupffer cells, the most abundant tissue macrophages, are originated from yolk sac-derived cells. They are essential for hepatic and systemic homeostasis. [21] Understanding how NPs interact with Kupffer cells is critical to developing more effective nanomedicines. Ergen et al. compared the cellular distributions of 10 nm poly(N-(2-hydroxypropyl) methacrylamide) polymers, 100 nm PEGylated liposomes and 2 μm poly(butyl cyanoacrylate) microbubbles in different organs *via* intravital multi-photon microscopy [22]. All nanoparticles had similar organ-level accumulation in the liver and spleen, while having dramatic differences in their cellular distribution within the liver. Prior to nanoparticle administration, Kupffer cells were labelled by injection of latex microspheres. Microbubbles were shown to rapidly and almost exclusively be captured from circulation by these latex microsphere labelled Kupffer cells within the first 30 min after microbubble administration. A few singular agglomerates traversing vessels, which were likely monocytes carrying microbubbles, were also observed. Injection of liposomes initially led to a high intravascular signal, after which the liposomes were found to gradually accumulate in liver Kupffer and endothelial cells over a period of 2 h. In contrast, polymeric nanoparticles primarily remained within the vasculature for the first 2 h, showing only minor uptake by endothelial cells. Moreover, mannose-decorated polymeric NPs showed higher uptake in endothelial cells as well as by CD206^{+} Kupffer cells, compared to non-decorated polymeric NPs. In another study, "off/on" NPs with a pomegranate-like structure and a size of ~400 nm were developed to specifically target Kupffer cells [23]. These NPs were used to monitor the spatial distribution of Kupffer cells along the central vein (CV)−portal triad (PT) axis, providing further insights in liver physiology.

2.2.3. Tumor-associated macrophages (TAMs)

Targeting TAMs is an active anti-cancer strategy for nanomedicine. There are two main phenotypes of TAMs: M1 and M2 macrophages. Advances in M1/M2 macrophage-NP interactions have been reviewed in detail [24]. Here we highlight one example of iron oxide NP-TAM interaction in the 4T1-GFP tumour microenvironment, which was reported by Efremova et al. As soon as 15 min after injection, Cy5-labelled Fe_3O_4-Au NPs were detected outside tumour vessels. Over time, the accumulation of these NPs was shown to increase, but was limited to the 100 μm perivascular region. Of note, the release dynamics of payload from the NPs differed from the distribution of NPs themselves. Nile Red was non-covalently loaded into the polymeric shell of Fe_3O_4 NPs, mimicking the loading of a hydrophobic drug (*e.g.* paclitaxel). Real-time imaging revealed that Nile Red was released rapidly in the tumour microenvironment within just 2 min after NP attachment to the vessel wall .The difference in distribution between carrier and cargo may be due to the non-covalent loading method used, which can cause the release of the cargo to be sensitive to physical forces within the local environment, thus leading to a quick release [25]. The selective uptake of LiLa particles in M1 macrophages within inflamed adipose tissue has also been demonstrated by single-photon intravital imaging in mice [26]. Rhodamine-labelled ferumoxytol, clinically applicable iron oxide nanoparticles, have been utilized for endogenous labelling of macrophages for detection of immune responses to stem cell transplants [27]. Intravital microscopy confirmed the uptake of ferumoxytol NPs in macrophages, as evidenced by their fluorescence colocalization in the skull defects of transgenic mice with window chambers.

Monocytes/macrophages, which belong to the MPS, enable internalization of particles, present antigens to the adaptive immune

Table 1
Understanding nanoparticle-cell interactions *via* intravital imaging.

NPs	Type	Dye Labelling	Shape	Size (nm)	Surface modification	Charge (mv)	Time, Cells	Ref.
Fe_3O_4 nanoparticles	Inorganic	Cy5	Cube	139.6 ± 63	PEG	−9.1	Immediately after i.v. injection, Neutrophils ($CD11c^+Ly6G^+$)	[11]
Fe_3O_4 nanoparticles	Inorganic	Cy5	Cluster	139.7 ± 56	PEG	−11.2	Immediately after i.v. injection, Neutrophils ($CD11c^+Ly6G^+$)	[11]
Carboxylated polystyrene nanoparticles	Organic	Cy5	Spherical	115~140	BSA-modified, PEG	−25~−35	30 min post i.v. injection, Neutrophils ($Gr\text{-}1^+$) with TNF-α stimulation	[12]
Carboxylate and neutravidin-labelled nanoparticles	Organic	Yellow-green fluorescent (505 / 515)	Spherical	232.1	CD11b antibody-decorated, PEG	−13.5	3 h after i.v. injection, Neutrophils ($Ly6G^+$) with PS stimulation	[13]
Gold nanoparticles	Inorganic	n/a	Rod	50 × 150	CD11b antibody-decorated, PEG	−10~−15	n/a, Neutrophils ($Ly6G^+$) with PS stimulation	[13]
Neutrophil membrane nanovesicles	Organic	DiO/ DiL	Spherical	200	n/a	−16/ −14	n/a, Neutrophils (Gr-1) with TNF-α stimulation	[14]
Single-walled carbon nanotubes (SWNTs)	Inorganic	Cy5.5	Tube	1.2 × 150	With/ without RGD conjugated, PEG	n/a	2 h, 6 h (i.v.) Monocytes ($Ly\text{-}6C^{hi}$ $CD11b^+$)	[7]
Lipid-based nanoparticles (7C1/siRNA-CX3CL3)	Organic	Alexa 647	Spherical	35~60	PEG	Neutral	n/a, Endothelial cells-Monocytes ($CX3CR1^+Ly\text{-}6C^{low}$)	[19, 20]
Poly Microbubbles	Organic	Rhodamine-B and 1,1,3,3,3,3-hexamethylindotricarbocyanine (HITC) iodide	Spherical	2000	n/a	n/a	Within 30 min (i.v.), Kupffer cells	[22]
Nano pomegranate-like nanoparticles	Organic	DiR-BOA	Spherical	400	n/a	n/a	2 h (i.v.), Kupffer cells ($F4/80^{high}$ $CD11b^{int}$)	[23]
Poly(N-(2-hydroxypropyl) methacrylamide) Polymers	Organic	ATTO 488 and Dy750	Spherical	10	Mannose-decorated	n/a	Within 2 h (i.v.), Endothelial cells and Kupffer cells	[22]
Liposomes	Organic	Alexa Fluor 750, Alexa Fluor 488	Spherical	100	PEG	n/a	Within 2 h (i.v.), Kupffer cells and endothelial cells	[22]
Fe_3O_4-Au Janus nanoparticles	Inorganic	Cy5, NRed	Bulk-like	125~172	PEG	−20.2~−24.9	15~60 min (i.v.), tumour-associated macrophages	[25]
Hybrid lipid−latex (LiLa) nanoparticles	Organic	Alexa Fluor 647	Spherical	45~92	Phosphatidylserine (PtdSer) and cholesterol-9-carboxynonanoate (9-CCN) coated ,PEG	n/a	20 min after i.v. injection, M1 macrophages ($Ly6C^+F4/80^+$and c-fms^{YFP+} mice)	[26]

(*continued on next page*)

Table 1 (*Continued*)

NPs	Type	Dye Labelling	Shape	Size (nm)	Surface modification	Charge (mv)	Time, Cells	Ref.
Ferumoxytol (Clinically applicable Fe_3O_4 nanoparticles)	Inorganic	Rhodamine	Spherical	17−31	Polyglucose sorbitol carboxymethylether (PSC) coating	`~−16	Day 1-Day 21 (i.v.), Macrophages (Jax C57BL/6-Tg (Csf1r-EGFP-NGFR/FKBP1A/TNFRSF6) 2Bck/J mice)	[27]
Transferrin conjugated Liposomes	Organic	Cy5.5	Spherical	137 nm	PEG	−12.1	Imaging at 24 h (i.v.), Brain capillary endothelial cells	[28]
Transferrin conjugated Polymers	Organic	Nile red	Spherical	100−150	PEG	Positive	Imaging at 3 h (i.v.), Brain capillary endothelial cells	[29]
Poly(N-(2-hydroxypropyl) methacrylamide) Polymers	Organic	ATTO 488 and Dy750	Spherical	10	n/a	n/a	Within 2 h (i.v.), LSECs (minor)	[22]
Quantum dots	Inorganic	n/a	Spherical	2.1	n/a	−52	Within 3 h (i.v.), LSECs,	[31]
Peptide-lipid nanoparticles	Organic	DiR-BOA	Spherical	20	Peptide RXR or RXXR sequences decorated	Neutral	Seconds after i.v. injection, LSECs	[32]
Calciprotein particles	Organic	Alexa Fluor 488	Spherical	50−100	Fetuin-A protein mineral complexes	n/a	< 1 min (i.v.), LSECs	[34]
Few-atom gold nanoclusters	Inorganic	n/a	Cluster	<1	n/a	n/a	6 s, 3 min (i.v.) Endothelial cells	[30]
1,2-diaminocyclohexane-platinum(II) (DACHPt) based Polymers	Organic	Alexa Fluor 647	Spherical	30,70	n/a	n/a	Eruptions occur stochastically throughout the 10 h (i.v.), Tumour endothelial cells (inter-endothelial gaps)	[8]
DOXIL (doxorubicin HCl liposomes)	Organic	n/a	Spherical	85	PEG	Neutral	Eruptions occur stochastically throughout the 10 h (i.v.), Tumour endothelial cells (inter-endothelial gaps)	[8]
Gold nanoparticles	Inorganic	Alexa Fluor 647	Spherical	50	PEG	n/a	0−85 min (i.v.), Tumour endothelial cells (GSL1-Cy3) (intra-endothelial)	[9]
Liposomes	Organic	DiD, DiO	Spherical	109±28	PEG	Neutral	Macropleakages were not stable in space and time (i.v.), Tumour endothelial cells (CD31)-Neutrophils (Ly6G)	[53]
SiO2 nanoparticles	Inorganic	Pacific blue	Spherical	70	PEG	n/a	Macrophages: within minutes Scavenger endothelial cells: with a time scale	[54]

(*continued on next page*)

Table 1 (*Continued*)

NPs	Type	Dye Labelling	Shape	Size (nm)	Surface modification	Charge (mv)	Time, Cells	Ref.
							of hours in transgenic zebrafish embryos(*fli1a:eGFP/ mpeg1:mCherry*)	
Amorphous silica nanoparticles	Inorganic	Red (569 / 585)	Spherical	50	n/a	Negative	2 min, 1 h after instillation, alveolar epithelial cells	[47]
Fe_3O_4 nanoparticles	Inorganic	Cy5	Cube, Cluster	140	PEG	Negative	Within 60 min (i.v.), Renal tubular epithelial cells	[48]
PLGA based nanoparticles	Organic	Cy5	Spherical	347.6 ± 21.0	PEG	−19.0 ± 0.3	72 h after injection (i.v.), Renal tubular epithelial cells	[49]
Ferumoxytol modified nanoparticles	Inorganic	FITC	Spherical	25.33 33 ± ± 1.70	DEVD peptide conjugated, PEG	−3.69 ± −1.29	Day1-Day 6 Labelling mouse mesenchymal stem cells and pig mesenchymal stem cells *in vitro*	[50]
Peptide and aptamer dual-functionalized nanoparticles	Organic	DiD, DiR	n/a	106~122	K237 peptide, Ep23 aptamer modified	−25.4~−31.4	Within 30 min, Circulating tumour cells (CTC)	[52]
Cowpea mosaic virus (CPMV) nanoparticles	Organic	Alexa Fluor 647	Spherical	30	E7p72 peptides decorated, PEG	n/a	Over 1.5 h, Tumour endothelial cells (Lectin rhodamine) in the avian embryo CAM	[36]
Mesoporous Silica supported lipid bilayers (Protocells)	Inorganic	Rhodamine B isothiocynate (RITC)	Hexagonal, spherical, rod-like	137−397	PEG	−4.0~−5.0	5 min, 30 min, 1 h, 4 h, 9 h; leukemia cells in the avian embryo CAM	[51]

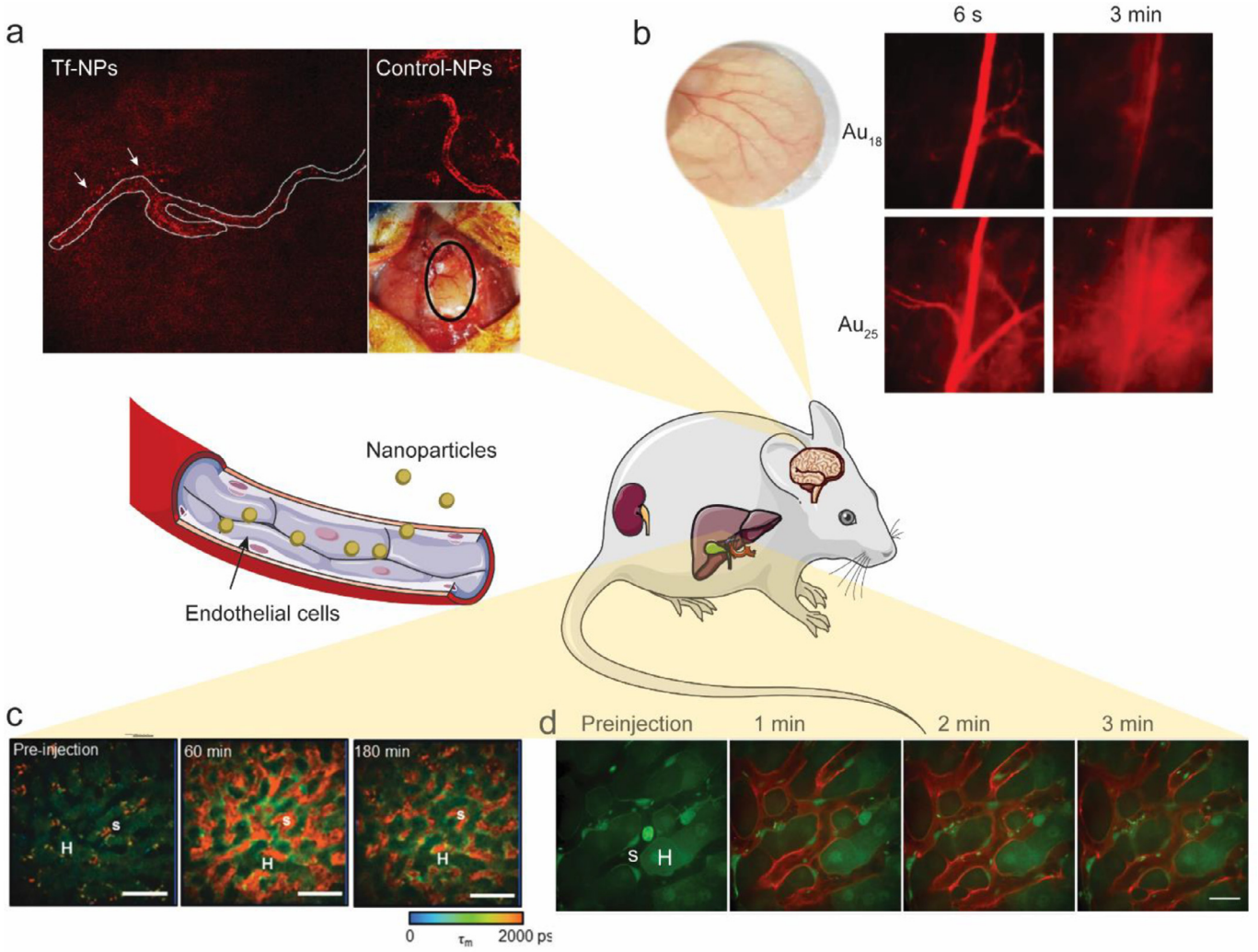

Fig. 1. Intravital imaging sheds light on nanoparticle-endothelial cell interactions. a) Transferrin-functionalized nanoparticles (Tf-NPs: transferrin-PEG2K-Cy5.5 liposomes) cross the intact BBB, while control-NPs (Hemagglutinin-PEG2K-Cy5.5 liposomes) do not. Modified from Lam et al. [28] with permission; b) Non-invasive bright-field and fluorescence images of mouse ear blood vessels 6 s and 3 min after i.v. injection of Au_{18} or Au_{25} clusters, showing that Au_{25} crossed the endothelium more rapidly than Au_{18}. Adapted from Du et al. [30] with permission; c) FLIM images of representative rat liver before, 60 min after, and 180 min after bolus injection of quantum dots (QD) with an emission channel of 515–620 nm. H represents the hepatocytes, while S represents the hepatic sinusoids. Adapted from Liang et al.[31] with permission; d) Intravital imaging of α-melittin-NPs in the liver showed that NPs quickly target LSECs. α-melittin-NPs were labeled with DiR-BOA (red), a lipid-anchored near-infrared fluorophore. Actb-EGFP mice were used to visualize the structure of the liver. Adapted from Yu et al. [32] with permission. (For interpretation of the references to color in this figure legend, the reader is referred to the web version of this article.)

system, secrete chemokine and cytokine mediators, exhibit cytotoxic activity against tumours [17], and interact with different sizes, shapes, and surface features of nanoparticles (Table 1). Understanding how NPs interact with these cells can aid in the design of long-circulating NPs, thus enhancing tumour uptake and improving anti-tumour efficacy.

2.3. IVM imaging of nanoparticle-endothelial cell interactions

After intravenous administration, NPs must interact with the blood endothelium in different tissues and tumours, either by transport through inter-endothelial gaps or *via* endothelial transcytosis or other unknown mechanisms. The kinetic process by which nanoparticles are transported across the vascular endothelium is a “hot” and debatable topic, and IVM imaging can provide insights that are not possible by other means.

2.3.1. Blood-brain barrier (BBB)

The majority of NPs are blocked by the blood-brain barrier (BBB) and are thus unable to enter the brain. Recently, IVM was used to show transport of transferrin-functionalized nanoparticles (Tf-NPs) across the BBB in non-tumour bearing mice [28]. Tf-NPs were composed of a 1,2-distearoyl-sn-glycero-3-phosphoethanolamine-N-[amino(polyethene glycol)−2000] (DSPE-PEG2K) linker conjugated with Cy5.5-transferrin. Intravital images demonstrated that Tf-NPs were transported across the endothelium of microvessels into the surrounding subarachnoid space in normal mice with intact BBBs (Fig. 1a). A diffusion gradient of NPs away from the blood vessel was observed. In mice with orthotopic brain tumours, Tf-NPs loaded with temozolomide and the bromodomain inhibitor JQ1 showed better tumour delivery and improved anti-tumour efficacy compared to those without transferrin modification. Similarly, anti-transferrin antibody functionalized chitosan nanoparticles were able to deliver caspase inhibitor and basic fibroblast growth factor across the BBB to provide neuroprotection [29]. Inhibition of vesicular transcytosis by imatinib abolished the brain permeation of these nanoparticles, further confirming transferrin receptor-mediated transcytosis.

2.3.2. Glomerular filtration membrane of kidneys and ear blood vessels

Particles smaller than 6 nm can readily pass the glomerular filtration barrier. A slight decrease in the particle size leads to a remarkable increase in the clearance efficiency for nanoparticles ranging

from 2 to 6 nm. Zheng's group gave a comprehensive review of different transport mechanisms of nanoparticles in the kidneys [33]. They also found that the glomerular filtration barrier significantly slowed down renal clearance of sub-nanometre gold nanoclusters (AuNCs) [30]. It appears that smaller AuNCs are more readily trapped by the glomerular glycocalyx than larger ones. A similar extravasation pattern was also observed in normal ear blood vessels, with Au_{25} crossing the endothelium more rapidly than Au_{18} (Fig. 1b). Image quantification showed that it took only 2.7 min for Au_{25} to reach an equilibrium between the tissue interstitial space and artery, while the intensity of Au_{18} in the tissue interstitial space was only 37% of that in the artery at the end of the same period.

2.3.3. Liver sinusoidal endothelial cell (LSEC)

Most NPs are trapped in the liver after intravenous injection. Liver sinusoidal endothelial cells (LSECs) line the capillary-sinusoids in the liver. Intravital imaging can be used to visualize NPs circulating in sinusoids or interacting with LSECs *in vivo*. Liang et al. investigated spatiotemporal disposition of negatively charged mercaptosuccinic acid (MSA)-capped cadmium telluride/cadmium sulfide (CdTe/CdS) quantum dots (QDs, 2.1 nm) in rat livers using multiphoton microscopy (MPM) coupled with fluorescence lifetime imaging (FLIM) [31]. In this technique, the fluorescence decay kinetics of each individual pixel are transformed into a spatial distribution of fluorescence lifetime. QDs have a longer fluorescence lifetime (typically $\geq$ 10 ns) than tissue autofluorescence (2−3 ns), which enables FLIM imaging to distinguish fluorophores from their environments in biological tissues. The images revealed that QDs (shown in red; Fig. 1c) with a longer lifetime component, $\tau 2$, are retained in the sinusoids and selectively taken up by sinusoidal cells (Kupffer cells and liver sinusoidal endothelial cells), but not by hepatocytes (shown in green; Fig. 1c) with a shorter lifetime component, $\tau 1$, within 3 h. Yu et al. utilized intravital imaging *via* spin-disk confocal microscopy to confirm that melittin nanoparticles targeted LSECs within seconds after injection (Fig. 1d). Actb-EGFP mice were used in this study to visualize the structure of the liver. α-melittin-NPs were found to trigger the activation of LSECs and switch the hepatic immunologic environment to the activated state. This fast timeline may be critical for immune modulation in the liver, leaving the NPs without any opportunity to contact or interact with other immunocytes in the hepatic sinusoids to induce any subsequent events [32]. Similar rapid (<1 min) LSEC uptake of NPs with a size of 50−100 nm was reported using fluorescent fetuin-A labelled colloidal protein-mineral complexes, known as primary calciprotein particles (CPP) [34].

2.3.4. Nanoparticle-endothelial cell interactions in tumours

How nanoparticles interact with endothelial cells in tumours is a crucial question to improve nanomedicie tumour uptake, accumulation, and retention. Intravital imaging can provide spatiotemporal information about nanoparticle distribution in the tumour and allow for new insights into their transport mechanisms.

Targeting neovasculature is an important strategy for anti-cancer treatment. Cowpea mosaic virus (CPMV) nanoparticles functionalized with RGD peptide were observed to accumulate in MDA-MB-468 human breast cancer tumours in the avian embryo chorioallantoic membrane over a period of 12 h [35]. Similarly, CPMV based nanoparticles were decorated with an EGFL7-binding peptide, E7p72, to specifically target tumour-associated neovasculature [36]. Real-time live intravital imaging of tumour neovasculature and normal blood vessels showed that CPMV-PEG-E7p72, but not CPMV-PEG control nanoparticles, accumulated in the tumor endothelium. Quantification of NP intensity indicated that the NPs quickly accumulated in the tumour neovasculature. Colocalization analysis between NPs and lectin further confirmed this tumour neovasculature targeting. The use of CPMV nanoparticles in cancer therapy and imaging, including intravital imaging, have been reviewed in detail [35].

The enhanced permeability and retention (EPR) effect is a central dogma for nanomaterial transport into solid tumours. In brief, tumour vasculature was believed to experience increased permeability due to the presence of large inter-endothelial gaps. Tumour vasculature leakage, poor lymphatic drainage, and slower blood flow in tumours are believed to provide small nanoparticles with the opportunity to pass through inter-endothelial gaps enhancing their passive diffusion and accumulation [37, 38]. The Kataoka group observed, using intravital imaging, that the EPR effect is not a static process. Instead, it exists as a dynamic vascular burst followed by a brief, vigorous outward flow of fluid (eruption) into the tumour interstitial space, with or without leukocytes nearby (Fig. 2a,2c). Harney et al. used IVM to demonstrate that $TIE2^{hi}$ /$VEGFA^{hi}$ perivascular macrophages are responsive to the transient vascular permeability in tumours [39]. However, no statistical relationship between the presence of vascular leukocytes and the occurrence of eruptions was found in Kataoka's study. They studied the permeability of tumour blood vessels using two different sizes (30 and 70 nm) of fluorescently labelled polymeric nanoparticles in both hypovascular human pancreatic BxPC3-GFP tumours and U87MG glioblastoma tumours. The eruptions were shown to occur stochastically throughout the 10 h observation period. Static permeability that is inherently mediated by the presence of small static pores was found to be a major factor for the uptake of smaller nanoparticles (30 nm), but not as much of a factor for the uptake of larger nanoparticles (70 nm). They concluded that smaller nanoparticles could utilize both eruption and static permeability across static pores, whereas larger nanoparticles and Doxil primarily rely on eruption. These findings offer a new image-guided optimization strategy for the design of larger NPs whose uptakes rely on the occurrence of dynamic vascular bursts rather than transport across static pores [8] The EPR effect has also shown promise in cardiovascular disease. Recently, Beldman et al. showed that antiglycolytic therapy induces vascular renormalization, leading to decreased vascular leakiness and reduced uptake of hyaluronan nanomaterials. This supports the role of vascular leakiness in the uptake of nanomaterials, and suggests that employing a vascular normalization therapeutic strategy should not be done in conjunction with NP delivery that relies on the EPR effect [40].

However, the reliance of EPR effect on inter-endothelial gaps was recently challenged by Chan's group. They found that these inter-endothelial gaps are not responsible for the transport of nanoparticles into solid tumours. Instead, an active process through endothelial cells (Fig. 2b) accounts for majority of NP entry into tumours. Four different mouse models: U87-MG, 4T1, PDX and MMTV-PyMT, along with three different types of human tumours were utilized for the analysis. Using a custom microlensed spinning disk confocal microscope, intravital imaging of MMTV-PyMT mice was conducted to observe the active transcytosis process of AuNPs. The images demonstrated colocalization of the NPs (labelled with Alexa Fluor 647) with endothelial cells to form hotspots along the vessel lining (red, stained with GSL1-Cy3) over time, which indicates interaction between the nanoparticles and endothelial cells (Fig. 2d). These spots are not transient. Transmission electron microscopy (TEM) further validated these spots in different stages of extravasation *via* transcytosis, *e.g.* uptake, vesicular localization and exit into the tumour interstitium [9]. Whether it is the inter-endothelial transport or intra-endothelial transport that contributes to the EPR effect remains a debate. More systematic studies that take into consideration the physicochemical properties of the nanoparticles, the shear stress by blood flow [41], stromal parameters such as fibroblasts [42], fluid convection and interstitial fluid pressure [43], as well as the resolution of microscopes [44], are needed to better understand the complicated tumour targeting behaviours of different types of nanomaterials.

Understanding how NPs dynamically interact with endothelial cells is essential in order to tailor the systemic delivery of NPs to tumours. Beyond the size, charge, and surface modifications, the

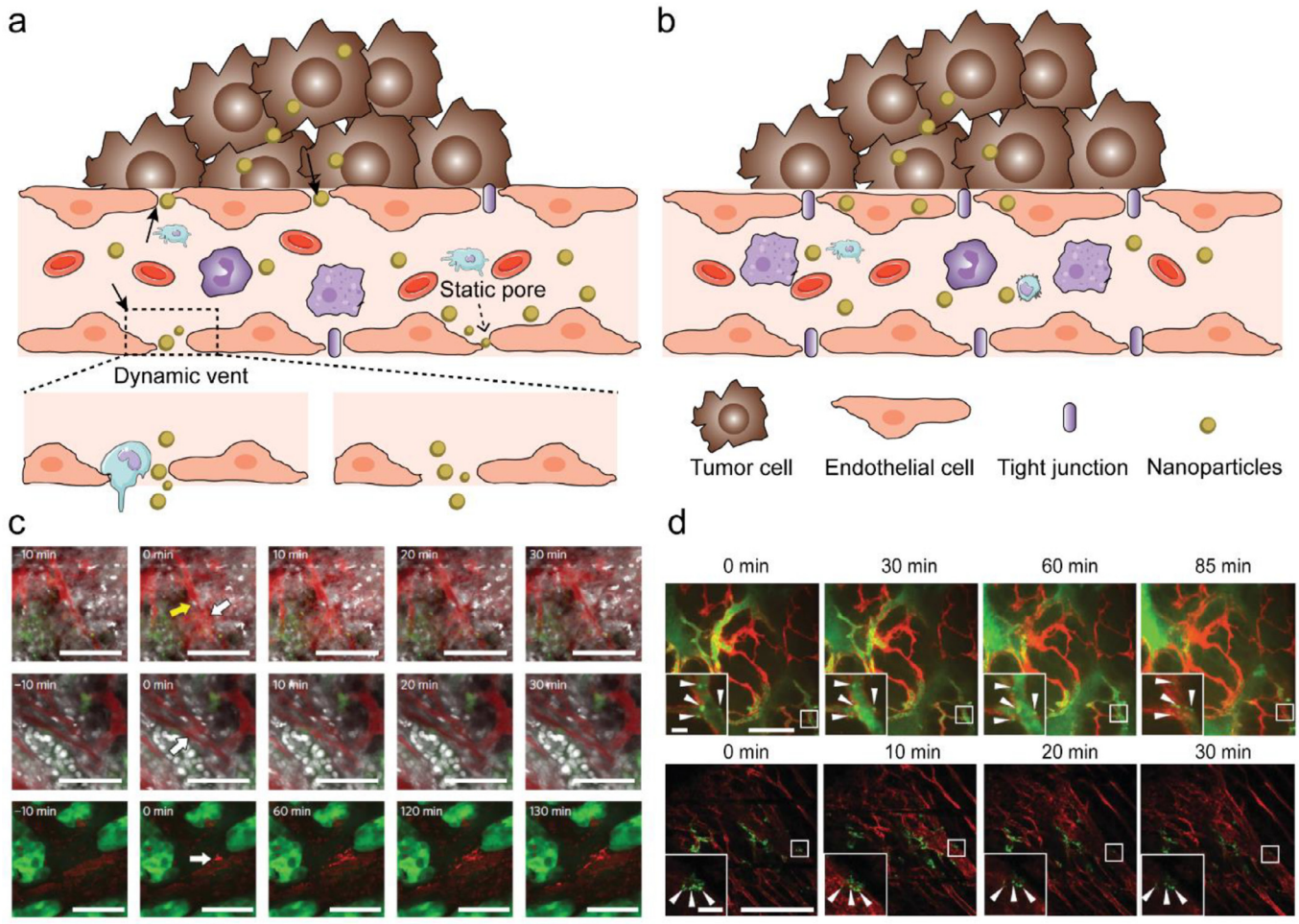

Fig. 2. New insights on EPR using IVM. a) NP transport through gaps between adjacent endothelial cells in dynamic vascular bursts; b) NP transport across the endothelial cell layer *via* transcytosis. c) Representative eruption (white arrow) occurring near a Hoechst-stained (white) leukocyte cell (yellow arrow) (top) and an eruption occurring without cells nearby(middle), respectively. 70 nm nanoparticles (red) and a BxPC3-GFP dorsal skinfold model (green) were used. Eruption of Doxil particles (red) using a GFP dorsal skinfold model (green) (bottom). Scale bars, 100 μm. Adapted from Matsumoto et al. [8] with permission; d) Intravital imaging shows colocalization of nanoparticles with endothelial cells to form hotspots along the vessel lining (red, stained with GSL1-Cy3). Arrows indicate hotspots. These vessels belong to MMTVPyMT (top) and 4T1 (bottom) tumour models. The 50 nm AuNPs (green) were conjugated with Alexa Fluor 647 to obtain the fluorescent signal. Scale bars, 200 μm; insets, 20 μm. Adapted from Sindhwani et al. [9] with permission. (For interpretation of the references to color in this figure legend, the reader is referred to the web version of this article.)

timing in which NPs transport through endothelial cells was largely ignored in the past. The early interactions between NPs and endothelial cells appear to play an important role in immune modulation. Thus, the order in which cells encounter NPs may also play a critical role in their delivery.

2.4. Other cell types

Another significant cell type that frequently interact with NPs are epithelial cells, which serve as physical barriers that prevent pathogens and toxins from entering the body. Choi et al. reported a rapid translocation of NPs from lungs to the draining mediastinal lymph nodes and the bloodstream after administration in lungs [45, 46]. *In vivo* clearance of amorphous silica nanoparticles by transcytosis across alveolar epithelial cells was visualized by IVM as well. The silica NPs, suspended in perfluorocarbon, were administered into the lungs of mice for imaging. NPs formed agglomerates that settled on the alveolar wall. Half of these agglomerates were removed from the lung within 30 min. Smaller agglomerates were observed to disappear quickly, whereas larger entities experienced a gradual reduction in size. A fraction of particle agglomerates remained stationary within the observation timeframe of 1 h, suggesting a second, slower phase of clearance [47].

Besides illustrating NP interactions with alveolar epithelial cells in the lung, intravital imaging has also shed light on how NPs interact with tubular epithelial cells in the kidney. Renal clearance is limited by glomerular basement membrane (GBM) pore size (~6 nm), although there is growing evidence that NPs exceeding this threshold can also be excreted through urine. Naumenko et al. conducted real-time tracking of Cy5-labelled PEGylated 140 nm iron oxide cubes and clusters in both the superficial renal cortex and renal tubules using IVM. Intravital imaging recorded NP transport from peritubular capillaries to the basal compartment of tubular cells, and subsequent excretion to the lumen within 60 min after systemic administration. The results suggest that translocation through the peritubular endothelium to tubular epithelial cells is an alternative mechanism of renal clearance, enabling excretion of NPs above the glomerular cut-off size [48]. The specific uptake of large diameter (350–400 nm) polymer-based mesoscale nanoparticles (MNPs) that targeted the renal proximal tubular epithelial cells has also been observed by IVM [49].

Intravital imaging has also recently been applied to study the interaction of NPs with other cells. For example, the *in vivo* fate of stem cells was evaluated by intravital imaging and magnetic resonance imaging (MRI) using a caspase-3 cleavable peptide-dye conjugated with clinically-approved ferumoxytol NPs [50]. They labelled both mouse mesenchymal stem cells and pig mesenchymal stem cells

with the NPs and then transplanted the labelled cells within biocompatible scaffolds to calvarial defects in mice. The immune response to transplantation of pig mesenchymal stem cells within the mice induced cleavage of the peptide-dye conjugate, triggering an increase in fluorescence intensity, allowing for detection of the immune response. Additionally, the ability of mesoporous silica NP-supported lipid bilayers (Protocells) to be delivered to individual leukaemia cells (REH leukaemia cell line transduced with EGFR) was observed *via* intravital imaging in chick embryo chorioallantoic membrane (CAM) [51]. Furthermore, the use of aptamer dual-functionalized nanoparticles (dTNP) to target and neutralize circulating tumour cells (CTC)-in the bloodstream of a 4T1-GFP cell-derived lung metastasis mouse model was demonstrated using *in vivo* flow cytometry (IVFC), intravital imaging, and confocal microscopy analysis [52]. Understanding the interaction of a variety of cells with NPs (Table 1) will better extend the application of NPs in the future.

2.5. Simultaneous interaction with multiple cell types

Once NPs are intravenously injected, they will encounter and interact with many different types of cells or subsets of cells *in vivo*. However, no cells are working in an isolated state in the real microenvironment of the body. The role of multiple cell types working in tandem on shaping NP delivery is an interesting topic, and some recent examples have started to address this issue.

2.5.1. NP-neutrophil-endothelial cell interactions

Liposomes are currently the most extensively used nanocarriers in anti-cancer treatment. Naumenko et al. utilized IVM to track 1,1′-dioctadecyl-3,3,3′,3′-tetramethylindodicarbocyanine (DiD)-labelled neutral liposomes (109 ± 28 nm) in xenograft tumour models (murine breast cancer 4T1, melanoma B16, human prostate cancer 22Rv1) and normal skin. The neutrophil and liposome extravasation dynamics were recorded as images (Fig. 3a). Importantly, their results were in contrast to previously depicted neutrophil-mediated delivery routes in which neutrophils directly engulf NPs before transporting them through the endothelium. In this study, the neutrophils did not take up liposomes directly. However, the decreased accumulation of liposomes in 4T1 tumours under a neutrophil-depleted state further indicated that these cells have a positive effect on NP delivery. Furthermore, intravital images found that extravasation spots were detected more frequently in the proximity of neutrophils. Thus, they proposed that two distinct extravasation patterns exist for liposome transport through the endothelium: microleakage and macroleakage. The former, a local perivascular nanoparticle deposition, was observed both in tumours and healthy tissues. This type of liposome leakage is not specific for tumours and is responsible for drug deposition in normal tissues. Instead, macroleakage mediated by neutrophils is the greatest contributor to tumour accumulation [53]. Thus, in this study, neutrophils promoted NP delivery to tumour tissue by collaborating with endothelial cells, leading to a macroleakage extravasation pattern.

2.5.2. NP-macrophage-endothelial cell interactions

In contrast to the collaborative relationship between neutrophils and endothelial cells for NP delivery, a competition between macrophages and endothelial cells was reported recently. Hayashi et al. performed three-colour intravital imaging using pacific blue-labelled model nanoparticles (70 nm SiO_2) in transgenic zebrafish embryos with cell type-specific fluorescent reporters (*fli1a:eGFP/mpeg1:mCherry*). In this model, the GFP fluorescence represented the signal from scavenger endothelial cells (SECs), while the mCherry fluorescence indicated the signal from macrophages. They found that macrophages rapidly sequestered nanoparticles *via* membrane adhesion and endocytosis (including macropinocytosis) within minutes after injection, while SECs trapped single nanoparticles *via* scavenger receptor-mediated endocytosis, resulting in gradual sequestration with a time scale of hours (Fig. 3b). Inhibition of the scavenger receptors *via* DexSO4 hindered SECs from accumulating nanoparticles (decreased from ~77% to ~22%) but enhanced uptake in macrophages (increased from ~2% to ~65%), indicating a competitive relationship between SECs and macrophages for nanoparticle clearance *in vivo*. The kinetics of nanoparticle sequestration in SECs and macrophages were assessed within the first 30 min post-injection *via* intravital imaging, and the image analysis further supports the rapid nanoparticle accumulation by macrophages and gradual sequestration by SECs with slower kinetics but a more profound contribution to the overall blood clearance. One limitation of this study is that as the macrophage: SECs ratio is a critical factor to determine their respective contributions in a given tissue, the difference between zebrafish embryos (1:10) and the mammalian liver (roughly 1:2,3) may lead to a different conclusion in other models [54].

2.6. Understanding spatiotemporal NP-cell interactions under stimulation in vivo

To accelerate clinical translation of cancer nanomedicine, in addition to optimizing physicochemical properties of NPs, tumor microenvironment modulation strategies (for example radiation stimulation, ultrasound stimulation, and photodynamic therapy (PDT)) have been applied in order to improve tumor uptake. In this section, we will discuss how these stimulations change the behavior of NP transport, as revealed by intravital imaging.

2.6.1. Radiation therapy (RT) and radiofrequency (RF) ablation

High-resolution intravital imaging in HT1080 human fibrosarcoma-bearing mice with dorsal window chambers revealed that after radiation, tumour associated macrophages elicit dynamic bursts of extravasation, subsequently enhancing drug uptake in neighbouring tumour cells [55]. Fluorescent dextran was used to label the tumour vasculature. Dextran-coated 20-nm nanoparticles (NPs) were administered to $MerTK^{GFP/+}$fluorescent reporter mice (used to visualize TAMs), as well as transgenic mice with a nuclear-localizing 53BP1-mApple reporter protein (used to visualize tumour cells), 24 h before imaging. Images revealed that RT-treated mice have larger tumour vessels and more TAMs located near the vessels. In addition, cellular analysis of tumour imaging confirmed that the number of macrophages increased by >50% after RT and tumour cell density decreased correspondingly. Clinically relevant NPs (fluorescently labelled liposomes, polymeric micelles, and DOXIL) were all detected at higher concentrations in RT-treated tumours. However, no difference was observed between irradiated and unirradiated tumours in TAM-depleted mice, which further confirmed this TAM-dependent route. Lastly, combining radiation and cyclophosphamide led to enhanced vascular bursting and up to a six-fold increase of NP accumulation in tumours. Moreover, Lapin et al. found that non-invasive RF-induced mild (40−42 °C) hyperthermia can significantly enhance the extravasation of a water-soluble and fluorescent fullerene derivative (C60-serPF). Analysis of influx velocity and time indicated that C60-serPF had greater extravasation into orthotopic breast tumour tissue than into contralateral mammary fad pads [56]. The focal hyperthermia destruction induced *via* RF in tumour vessels may be a reason for this enhanced extravasation [57]. The same group provided a detailed protocol for the safe integration of intravital imaging with a high-powered non-invasive radiofrequency field applied to 4T1 orthotopic breast tumours in live mice [58].

2.6.2. Photodynamic therapy (PDT)

Like the TAM-dependent enhanced drug uptake caused by radiation therapy, Huis In 't Veld et al. demonstrated a tumour-associated myeloid cell-dependent enhancement of NP uptake in response to photodynamic therapy [59]. PDT increased the tumour accumulation of systemically administered lipid-PEG layer coated poly (lactic-co-

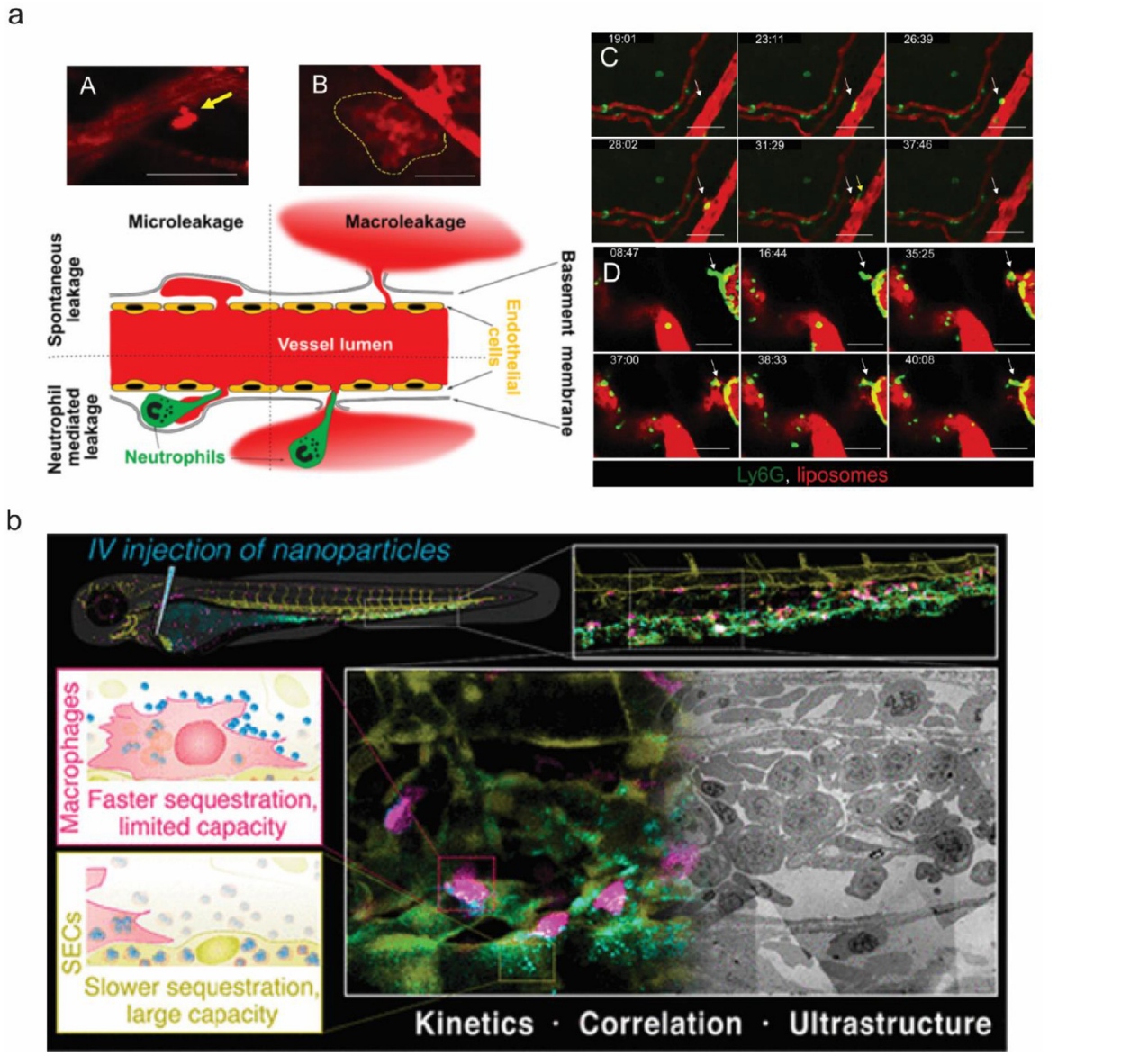

Fig. 3. The collaborative and competitive relationship between NPs and cells. a) IVM reveals two different liposome extravasation patterns. A-B. Representative images of liposome extravasation in 4T1 orthotopic tumors through microleakage (A, arrow) and macroleakage (B, dashed line) after i.v. injection. Time-lapse imaging of neutrophil extravasation followed by microleakage (C, arrow) and macroleakage development (D,arrow); red, liposomes; green, Ly6G-positive cells; scale bar, 50 μm. Yellow arrow in C points to an extravasated neutrophil crawling in the perivascular area. Adapted from Naumenko et al. [53] with permission; b) Faster nanoparticle sequestration by macrophages with limited capacity and slower nanoparticle sequestration *via* SECs with large capacity, visualized *in vivo* in real-time and at ultrastructural resolution. Adapted from Hayashi et al. [54] with permission. (For interpretation of the references to color in this figure legend, the reader is referred to the web version of this article.)

glycolic acid) (PLGA) nanoparticles. Intravital microscopy and histological analysis of the tumour area revealed that the tumour vasculature was disrupted after PDT, leading to disturbed blood flow and the entrapment of nanocarriers at the tumour site. They observed that the nanoparticles that accumulated after treatment localized to cells present throughout the tumour site, and further analysis with flow cytometry confirmed that these cells were tumor-associated myeloid cells. Tumour accumulation increased *via* PDT may rely on at least two factors. The first is the direct change of vascular structure. In our previous work, we observed enlarged fenestrae on the endothelial walls in PDT-treated mice [60]. The second factor is that PDT can also deconstruct the extracellular matrix (ECM), which hinders NP penetration [61].

2.6.3. Ultrasound (US) stimulation

Another technique for vascular disruption is the acoustic vaporization of micro- or nanoscale droplets (MDs or NDs) induced by ultrasound sonication. The intravital penetration of DiI-labelled liposomes was observed using an acousto-optical integrated system with a 2-MHz focused ultrasound transducer in a window-chamber mouse model. In the intravital image analyses, the intratumoral accumulations of DiI-labeled liposomes were 1.7- and 2.3-fold higher in the MD and ND groups treated with ultrasound than in groups that were not treated with ultrasound [62]. Similarly, intravital imaging provided direct visualization of disrupted tumour vessels (vessel size $<$ 30 μm). The extravasation distance under ultrasound was increased 8.3-fold compared to mice treated with DOX-nanodroplets alone [63]. For the extravasation distance, significant variations in the extracellular matrix have also been observed. Extravasation distance was dependent on many factors, such as mechanical indexes (MI). At higher MI, the extravasation occurred in smaller vessels and was more likely to occur close to vessel branching points. US also altered NP flow velocity and blood flow direction in an MI-dependent manner [64]. Besides the extravasation distance, the rate of diffusion is also critical for NPs accumulation. Ultrasound enhanced the

extravasation of micelles 1.5-fold and that of nanodroplets 4.7-fold, and a faster extravasation and tumour cell internalization occurred for polymeric micelles than nanoemulsion droplets. An extra-fast diffusion should be avoided as it may result in the flow of extravasated nanoparticles from the tumour to healthy organs [65]. Moreover, unlike imaging with MDs or NDs only, an ultrasound-triggered conversion of high payload porphyrin-encapsulated microbubbles to nanobubbles was monitored by simultaneous intravital and acoustic imaging. Rapid extravasation of the agent occurred in less than two minutes. Of note, this provides direct evidence of extravascularly intact nanobubbles obtained by taking advantage of simultaneous dual-modality imaging [66].

Stimulations including radiation, PDT, and ultrasound are all able to enhance extravasation of NPs in tumours through changing vascular structure/function or deconstructing the ECM, thus achieving better tumour accumulation of NPs.

3. Outstanding questions and future perspectives

Intravital microscopy has provided valuable new insights into the fundamental interactions between nanoparticles and cells. These insights have included providing a better understanding of the controversial EPR hypothesis, illustrating the competition between different cell types for nanoparticle uptake, and demonstrating that various cell types can play an active role in nanoparticle transport to tissues of interest. There are a number of factors that must be taken into consideration for expanded use of IVM in studying nanoparticle-cell interactions. First, the development of high-throughput and standardized IVM techniques, such as those described by Miller et al. [67] can provide a structured approach that can be widely adopted across multiple labs. This can allow for greater reproducibility and comparability of results, especially through the adoption of quantitative methods [68]. Second, considering the potential physiological differences between animal models and humans, the adoption of IVM for *in vivo* human use where possible can provide a more accurate understanding of nanoparticle interactions with human tissue. For example, a recent report by Mohammed et al. used multiphoton tomography with fluorescence lifetime imaging microscopy to demonstrate the safety of ZnO NPs as a widely used broad-spectrum sunscreen in humans [69]. Third, insights provided by IVM studies should be adapted in the design of nanomedicines. It is clear that nanoparticle features such as size, composition, and surface functionalization play an important role in interactions between nanoparticles and tissues of interest. In addition, the tissue microenvironment can be primed for more favorable nanoparticle uptake through the application of various stimuli. These parameters should be considered and can be extensively explored with specific particle systems and diseases in mind, allowing for optimization of nanoformulations based on a thorough understanding of the tissue microenvironment.

4. Search strategy and selection criteria

Data for this review were identified by searches of PubMed, and references from relevant articles using the search terms “nanoparticles”, “intravital imaging”, and/or “*in vivo* imaging” between 2015 and 2020 were included.

Declaration of Competing Interest

The authors declare that there are no conflicts of interest.

Acknowledgements

Research relevant for this review was supported by the Intramural Research Program, National Institute of Biomedical Imaging and Bioengineering, National Institutes of Health.

References

[1] Anselmo AC, Mitragotri S. Nanoparticles in the clinic: an update. Bioeng Transl Med 2019;4(3):e10143.
[2] Mitragotri S, Anderson DG, Chen X, Chow EK, Ho D, Kabanov AV, et al. Accelerating the translation of nanomaterials in biomedicine. ACS Nano 2015;9(7):6644–54.
[3] Wilhelm S, Tavares AJ, Dai Q, Ohta S, Audet J, Dvorak HF, et al. Analysis of nanoparticle delivery to tumours. Nat Rev Mater 2016;1(5):16014.
[4] Miller MJ, Wei SH, Parker I, Cahalan MD. Two-photon imaging of lymphocyte motility and antigen response in intact lymph node. Science 2002;296(5574):1869–73.
[5] Stoll S, Delon J, Brotz TM, Germain RN. Dynamic imaging of T cell-dendritic cell interactions in lymph nodes. Science 2002;296(5574):1873–6.
[6] Huang Q, Cohen MA, Alsina FC, Devlin G, Garrett A, McKey J, et al. Intravital imaging of mouse embryos. Science 2020;368(6487):181–6.
[7] Smith BR, Ghosn EE, Rallapalli H, Prescher JA, Larson T, Herzenberg LA, et al. Selective uptake of single-walled carbon nanotubes by circulating monocytes for enhanced tumour delivery. Nat Nanotechnol 2014;9(6):481–7.
[8] Matsumoto Y, Nichols JW, Toh K, Nomoto T, Cabral H, Miura Y, et al. Vascular bursts enhance permeability of tumour blood vessels and improve nanoparticle delivery. Nat Nanotechnol 2016;11(6):533–8.
[9] Sindhwani S, Syed AM, Ngai J, Kingston BR, Maiorino L, Rothschild J, et al. The entry of nanoparticles into solid tumours. Nat Mater 2020;19(5):566–75.
[10] Németh T, Sperandio M, Mócsai A. Neutrophils as emerging therapeutic targets. Nat Rev Drug Discov 2020;19(4):253–75.
[11] Naumenko V, Nikitin A, Garanina A, Melnikov P, Vodopyanov S, Kapitanova K, et al. Neutrophil-mediated transport is crucial for delivery of short-circulating magnetic nanoparticles to tumors. Acta Biomater 2020;104:176–87.
[12] Chu D, Gao J, Wang Z. Neutrophil-Mediated Delivery of Therapeutic Nanoparticles across Blood Vessel Barrier for Treatment of Inflammation and Infection. ACS Nano 2015;9(12):11800–11.
[13] Chu D, Dong X, Zhao Q, Gu J, Wang Z. Photosensitization Priming of Tumor Microenvironments Improves Delivery of Nanotherapeutics via Neutrophil Infiltration. Adv Mater 2017;29(27):1701021.
[14] Gao J, Chu D, Wang Z. Cell membrane-formed nanovesicles for disease-targeted delivery. J Control Release 2016;224:208–16.
[15] Wang Z. Imaging Nanotherapeutics in Inflamed Vasculature by Intravital Microscopy. Theranostics 2016;6(13):2431–8.
[16] Weissleder R, Nahrendorf M, Pittet MJ. Imaging macrophages with nanoparticles. Nat Mater 2014;13(2):125–38.
[17] Lavoie PM. Levy O.125 - Mononuclear phagocyte system editors. In: Polin RA, Abman SH, Rowitch DH, Benitz WE, Fox WW, editors. Fetal and neonatal physiology. Fifth Edition Elsevier; 2017. p. 1208–16.
[18] Flores AM, Hosseini-Nassab N, Jarr K-U, Ye J, Zhu X, Wirka R, et al. Pro-efferocytic nanoparticles are specifically taken up by lesional macrophages and prevent atherosclerosis. Nat Nanotechnol 2020;15(2):154–61.
[19] Jung K, Heishi T, Khan OF, Kowalski PS, Incio J, Rahbari NN, et al. Ly6Clo monocytes drive immunosuppression and confer resistance to anti-VEGFR2 cancer therapy. J Clin Invest 2017;127(8):3039–51.
[20] Dahlman JE, Barnes C, Khan OF, Thiriot A, Jhunjunwala S, Shaw TE, et al. *In vivo* endothelial siRNA delivery using polymeric nanoparticles with low molecular weight. Nat Nanotechnol 2014;9(8):648–55.
[21] Krenkel O, Tacke F. Liver macrophages in tissue homeostasis and disease. Nat Rev Immunol 2017;17(5):306–21.
[22] Ergen C, Heymann F, Al Rawashdeh W, Gremse F, Bartneck M, Panzer U, et al. Targeting distinct myeloid cell populations *in vivo* using polymers, liposomes and microbubbles. Biomaterials 2017;114:106–20.
[23] Lin Q, Deng D, Song X, Dai B, Yang X, Luo Q, et al. Self-Assembled "Off/On" nanopomegranate for in vivo photoacoustic and fluorescence imaging: strategic arrangement of Kupffer cells in mouse hepatic lobules. ACS Nano 2019;13(2):1526–37.
[24] Kapitanova KS, Naumenko VA, Garanina AS, Melnikov PA, Abakumov MA, Alieva IB. Advances and challenges of nanoparticle-based macrophage reprogramming for cancer immunotherapy. Biochemistry (Mosc) 2019;84(7):729–45.
[25] Efremova MV, Naumenko VA, Spasova M, Garanina AS, Abakumov MA, Blokhina AD, et al. Magnetite-Gold nanohybrids as ideal all-in-one platforms for theranostics. Sci Rep 2018;8(1):11295.
[26] Bagalkot V, Badgeley MA, Kampfrath T, Deiuliis JA, Rajagopalan S, Maiseyeu A. Hybrid nanoparticles improve targeting to inflammatory macrophages through phagocytic signals. J Control Release 2015;217:243–55.
[27] Daldrup-Link HE, Chan C, Lenkov O, Taghavigarmestani S, Nazekati T, Nejadnik H, et al. Detection of stem cell transplant rejection with Ferumoxytol MR imaging: correlation of MR imaging findings with those at intravital microscopy. Radiology 2017;284(2):495–507.
[28] Lam FC, Morton SW, Wyckoff J, Vu Han TL, Hwang MK, Maffa A, et al. Enhanced efficacy of combined temozolomide and bromodomain inhibitor therapy for gliomas using targeted nanoparticles. Nat Commun 2018;9(1):1991.
[29] Yemisci M, Caban S, Fernandez-Megia E, Capan Y, Couvreur P, Dalkara T. Preparation and characterization of biocompatible chitosan nanoparticles for targeted brain delivery of peptides. Methods Mol Biol 2018;1727:443–54.
[30] Du B, Jiang X, Das A, Zhou Q, Yu M, Jin R, et al. Glomerular barrier behaves as an atomically precise bandpass filter in a sub-nanometre regime. Nat Nanotechnol 2017;12(11):1096–102.
[31] Liang X, Grice JE, Zhu Y, Liu D, Sanchez WY, Li Z, et al. Intravital multiphoton imaging of the selective uptake of water-dispersible quantum dots into sinusoidal liver cells. Small 2015;11(14):1711–20.

[32] Yu X, Chen L, Liu J, Dai B, Xu G, Shen G, et al. Immune modulation of liver sinusoidal endothelial cells by Melittin nanoparticles suppresses liver metastasis. Nat Commun 2019;10(1):574.
[33] Du B, Yu M, Zheng J. Transport and interactions of nanoparticles in the kidneys. Nat Rev Mater 2018;3(10):358–74.
[34] Koppert S, Buscher A, Babler A, Ghallab A, Buhl EM, Latz E, et al. Cellular clearance and biological activity of calciprotein particles depend on their maturation state and crystallinity. Front Immunol 2018;9:1991.
[35] Beatty PH, Lewis JD. Cowpea mosaic virus nanoparticles for cancer imaging and therapy. Adv Drug Deliv Rev 2019;145:130–44.
[36] Cho CF, Yu L, Nsiama TK, Kadam AN, Raturi A, Shukla S, et al. Viral nanoparticles decorated with novel EGFL7 ligands enable intravital imaging of tumor neovasculature. Nanoscale 2017;9(33):12096–109.
[37] Gerlowski LE, Jain RK. Microvascular permeability of normal and neoplastic tissues. Microvasc Res 1986;31(3):288–305.
[38] Matsumura Y, Maeda H. A new concept for macromolecular therapeutics in cancer chemotherapy: mechanism of tumoritropic accumulation of proteins and the antitumor agent smancs. Cancer Res 1986;46(12 Part 1):6387.
[39] Harney AS, Arwert EN, Entenberg D, Wang Y, Guo P, Qian BZ, et al. Real-time imaging reveals local, transient vascular permeability, and tumor cell intravasation stimulated by TIE2hi macrophage-derived VEGFA. Cancer Discov 2015;5(9):932–43.
[40] Kanthi Y, de la Zerda A, Smith BR. Nanotherapeutic shots through the heart of plaque. ACS Nano 2020;14(2):1236–42.
[41] Wang S, Chennupati R, Kaur H, Iring A, Wettschureck N, Offermanns S. Endothelial cation channel PIEZO1 controls blood pressure by mediating flow-induced ATP release. J Clin Invest 2016;126(12):4527–36.
[42] Golombek SK, May JN, Theek B, Appold L, Drude N, Kiessling F, et al. Tumor targeting via EPR: strategies to enhance patient responses. Adv Drug Deliv Rev 2018;130:17–38.
[43] Dewhirst MW, Secomb TW. Transport of drugs from blood vessels to tumour tissue. Nat Rev Cancer 2017;17(12):738–50.
[44] Gonschior H, Haucke V, Lehmann M. Super-resolution imaging of tight and adherens junctions: challenges and open questions. Int J Mol Sci 2020;21(3):744.
[45] Choi HS, Ashitate Y, Lee JH, Kim SH, Matsui A, Insin N, et al. Rapid translocation of nanoparticles from the lung airspaces to the body. Nat Biotechnol 2010;28(12):1300–3.
[46] Leiva-Juárez MM, Kolls JK, Evans SE. Lung epithelial cells: therapeutically inducible effectors of antimicrobial defense. Mucosal Immunol 2018;11(1):21–34.
[47] Detampel P, Ganguly A, Tehranian S, Green F, Singha S, Santamaria P, et al. *In vivo* clearance of nanoparticles by transcytosis across alveolar epithelial cells. PLoS ONE 2019;14(9):e0223339.
[48] Naumenko V, Nikitin A, Kapitanova K, Melnikov P, Vodopyanov S, Garanina A, et al. Intravital microscopy reveals a novel mechanism of nanoparticles excretion in kidney. J Control Release 2019;307:368–78.
[49] Williams RM, Shah J, Tian HS, Chen X, Geissmann F, Jaimes EA, et al. Selective nanoparticle targeting of the renal tubules. Hypertension 2018;71(1):87–94.
[50] Li K, Chan CT, Nejadnik H, Lenkov OD, Wolterman C, Paulmurugan R, et al. Ferumoxytol-based dual-modality imaging probe for detection of stem cell transplant rejection. Nanotheranostics 2018;2(4):306–19.
[51] Durfee PN, Lin YS, Dunphy DR, Muniz AJ, Butler KS, Humphrey KR, et al. Mesoporous silica nanoparticle-supported lipid bilayers (protocells) for active targeting and delivery to individual leukemia cells. ACS Nano 2016;10(9):8325–45.
[52] Yao J, Feng J, Gao X, Wei D, Kang T, Zhu Q, et al. Neovasculature and circulating tumor cells dual-targeting nanoparticles for the treatment of the highly-invasive breast cancer. Biomaterials 2017;113:1–17.
[53] Naumenko VA, Vlasova KY, Garanina AS, Melnikov PA, Potashnikova DM, Vishnevskiy DA, et al. Extravasating neutrophils open vascular barrier and improve liposomes delivery to tumors. ACS Nano 2019;13(11):12599–612.
[54] Hayashi Y, Takamiya M, Jensen PB, Ojea-Jimenez I, Claude H, Antony C, et al. Differential nanoparticle sequestration by macrophages and scavenger endothelial cells visualized in vivo in real-time and at ultrastructural resolution. ACS Nano 2020;14(2):1665–81.
[55] Miller MA, Chandra R, Cuccarese MF, Pfirschke C, Engblom C, Stapleton S, et al. Radiation therapy primes tumors for nanotherapeutic delivery via macrophage-mediated vascular bursts. Sci Transl Med 2017;9(392):eaal0225.
[56] Lapin NA, Krzykawska-Serda M, Dilliard S, Mackeyev Y, Serda M, Wilson LJ, et al. The effects of non-invasive radiofrequency electric field hyperthermia on biotransport and biodistribution of fluorescent [60]fullerene derivative in a murine orthotopic model of breast adenocarcinoma. J Control Release 2017;260:92–9.
[57] Nikfarjam M, Muralidharan V, Malcontenti-Wilson C, Christophi C. Progressive microvascular injury in liver and colorectal liver metastases following laser induced focal hyperthermia therapy. Lasers Surg Med 2005;37(1):64–73.
[58] Lapin NA, Krzykawska-Serda M, Ware MJ, Curley SA, Corr SJ. Intravital microscopy for evaluating tumor perfusion of nanoparticles exposed to non-invasive radiofrequency electric fields. Cancer Nanotechnol 2016;7:5.
[59] Huis In 't Veld RV, Ritsma L, Kleinovink JW, Que I, Ossendorp F, Cruz LJ. Photodynamic cancer therapy enhances accumulation of nanoparticles in tumor-associated myeloid cells. J Control Release 2020;320:19–31.
[60] Zhen Z, Tang W, Chuang Y-J, Todd T, Zhang W, Lin X, et al. Tumor vasculature targeted photodynamic therapy for enhanced delivery of nanoparticles. ACS Nano 2014;8(6):6004–13.
[61] Zhen Z, Tang W, Wang M, Zhou S, Wang H, Wu Z, et al. Protein nanocage mediated fibroblast-activation protein targeted photoimmunotherapy to enhance cytotoxic T cell infiltration and tumor control. Nano Lett 2017;17(2):862–9.
[62] Ho YJ, Chang YC, Yeh CK. Improving nanoparticle penetration in tumors by vascular disruption with acoustic droplet vaporization. Theranostics 2016;6(3):392–403.
[63] Ho YJ, Yeh CK. Concurrent anti-vascular therapy and chemotherapy in solid tumors using drug-loaded acoustic nanodroplet vaporization. Acta Biomater 2017;49:472–85.
[64] Yemane PT, Aslund AKO, Snipstad S, Bjorkoy A, Grendstad K, Berg S, et al. Effect of ultrasound on the vasculature and extravasation of nanoscale particles imaged in real time. Ultrasound Med Biol 2019;45(11):3028–41.
[65] Rapoport N, Gupta R, Kim YS, O'Neill BE. Polymeric micelles and nanoemulsions as tumor-targeted drug carriers: insight through intravital imaging. J Control Release 2015;206:153–60.
[66] Pellow C, O'Reilly MA, Hynynen K, Zheng G, Goertz DE. Simultaneous intravital optical and acoustic monitoring of ultrasound-triggered nanobubble generation and extravasation. Nano Lett 2020;20(6):4512–9.
[67] Miller MA, Weissleder R. Imaging the pharmacology of nanomaterials by intravital microscopy: toward understanding their biological behavior. Adv Drug Deliv Rev 2017;113:61–86.
[68] Ng TSC, Garlin MA, Weissleder R, Miller MA. Improving nanotherapy delivery and action through image-guided systems pharmacology. Theranostics 2020;10(3):968–97.
[69] Mohammed YH, Holmes A, Haridass IN, Sanchez WY, Studier H, Grice JE, et al. Support for the safe use of zinc oxide nanoparticle sunscreens: lack of skin penetration or cellular toxicity after repeated application in volunteers. J Invest Dermatol 2019;139(2):308–15.